ORIGINAL RESEARCH PAPER

Flexural uplift and magmatic underplating anomaly on the Argentine continental margin: profile at 43.5°S

Ana C. Pedraza De Marchi[1,2,4] · Marta E. Ghidella[3] · Claudia N. Tocho[4,5] · Juan R. Franzese[1,2,6]

Abstract

Magmatic underplating can be defined as the addition of mafic magma to the lower crust and uppermost mantle around the Moho. This phenomenon plays an important role in continental margins and other compressional and extensional tectonic environments. We have modeled the magmatic underplating effect using Process-Oriented Gravity Modeling (POGM) along a profile at 43.5°S on the Argentine continental margin, which re-thickens the crust and causes uplift. In POGM, the gravity anomaly is formed by the rift, sedimentation, and magmatic underplating anomaly. This work focuses on the flexural uplift produced by the magmatic underplating and its gravity anomaly, rarely investigated in margins since seismic refraction data is generally unavailable to the scientific community. Particularly, it has not been calculated in the volcanic sector of the Argentine continental margin before this work. The results yield an average maximum flexural uplift associated with magmatic underplating, which is um = 140.32 m ± 22.12 m, an average density of the underplated body of $\rho_x = 3133.89$ kg/m³ ± 22.71 kg/m³, and an average density of the sediment $\rho_s = 2207.78$ kg/m³ ± 42.58 kg/m³ and an average oceanic crustal thickness of 6.36 km. The average elastic thickness leaving out the magmatic underplating effect is Te = 24 km ± 2.02 km, and including it is Te = 33.89 km ± 2.35 km. The magmatic underplating anomaly has an opposite contribution to the typical free-air gravity edge-effect for the Airy and flexural cases.

Keywords Magmatic underplating · Process-Oriented Gravity Modeling · Flexural uplift · Argentine continental margin

✉ Ana C. Pedraza De Marchi
  cpedrazadm@cig.museo.unlp.edu.ar

1   Centro de Investigaciones Geológicas (CIG), La Plata, Buenos Aires, Argentina

2   Consejo Nacional de Investigaciones Científicas y Técnicas (CONICET), Buenos Aires, Argentina

3   Instituto Antártico Argentino (IAA), San Martín, Buenos Aires, Argentina

4   Facultad de Ciencias Astronómicas y Geofísicas (FCAG), Universidad Nacional de La Plata, La Plata, Buenos Aires, Argentina

5   Comisión de Investigaciones Científicas (CIC), Buenos Aires, Argentina

6   Facultad de Ciencias Naturales y Museo (FCNyM), Universidad Nacional de La Plata, Av. 122 y 60, La Plata, Buenos Aires, Argentina

Introduction

Magmatic underplating is the addition of mafic magma to the lower crust and uppermost mantle around the Moho, and many times it has been identified as a high-velocity body in seismic refraction lines (Franke et al. 2010). Magmatic underplating takes place in a wide range of tectonic settings and plays a significant role in the tectonomagmatic evolution of the lithosphere. Magmatic underplating is associated with compressional tectonic environments (e.g. magmatic arc and crust formation, underplating of the Precambrian crust) and extensional tectonic environments (e.g. big extensional areas, big sills and batholiths in transition zones of the Moho, rift zones, and volcanic continental margins) (Thybo and Artemieva 2013).

The origin of the magmatic underplating material is unknown, but researchers (Cox 1993; Thybo and Artemieva 2013) have suggested that it is generated at great depth in the mantle, which has risen due to its buoyancy (relative density differences between rising magma and surrounding rocks) and has been trapped near the Moho. Magmatic underplating

can cause crustal thickening when magma is cooled (Watts 2001a, b; Watts et al. 2009). Xenoliths of mantle material can be used to obtain data about the last magma source and reveal heterogeneities of magma mix and magma assimilation in depth (Beard and Ragland 2005). Scientific teams (e.g. Scheck-Wenderoth, M., Sobolev, S., Steinberger, B., Thomas, M., Trumbull, R., Weber, M., Yuan, X., GFZ-Potsdam) addressing Mantle Dynamics and Magmatic Processes have been researching into the thermo-mechanical behavior of the mantle and related magmatic processes. True time-dependent models for mantle flow beneath the South Atlantic and Africa have been evaluated using observational constraints from global tomography, potential temperature, magma composition, as well as dynamic topography evolution and subsidence histories (Scheck-Wenderoth and SAMPLE Group 2011). Explicit incorporation of mineral-phase changes, melting topologies, and melt migration/flow laws permit numerical simulation of magmatic processes for different boundary conditions (Scheck-Wenderoth and SAMPLE Group 2011).

The first evidence of magmatic underplating below the continental Moho is based on low resolution seismic and gravity data, which, in general, were in agreement with models of large continuous layers (e.g. Fowler et al. 1989). Seismic experiments of greater resolution have better imaged the structure of the magmatic underplating and mafic intrusions in the continental crust and have made advances in the general understanding of the involved processes (Franke et al. 2006, 2010). It is widely accepted that many passive volcanic rifted continental margins have been heavily underplated during the late stages of rifting and break-up (Thybo and Artemieva 2013).

Two end-member passive margin types (volcanic or magma-poor) are defined depending on the volumes of extension-related magmatism. Volcanic rifted margins are characterized by massive occurrences of extrusive volcanism over short time periods during breakup, manifested in seismic reflection data as seaward dipping reflectors (SDRs) (Franke 2013), and intrusive magmatism (magmatic underplating) created during the rupture of the continental lithosphere (Hinz 1981; White and Mckenzie 1989). Some reviews illustrate the wide distribution of such margins, representing 75–90% of the passive continental margins (Eldholm et al. 2000; Menzies et al. 2002).

The last phase of the break-up of Gondwana during the Late Jurassic and Early Cretaceous is associated with a complex history of rifting and magmatism on the conjugate continental margins of southern Africa and Argentine (Hinz et al. 1999). Hinz et al. (1999) showed that the sparsely investigated Argentine margin is volcanic. The volcanic characteristic of the Argentine margin and its South African conjugate is revealed by the extensive extrusive manifestations that form the South Atlantic Large Igneous Province (LIPs). These include the Parana (in Brazil) and Etendeka (in Namibia) Continental Flood Basalts and the offshore counterpart of extrusive complexes, represented by a voluminous volcanic wedge of seaward dipping reflections (SDRs). SDRs are extended along most of the outer Argentine and its conjugate from the South African margin (Blaich et al. 2009). Franke et al. (2007) made a detailed report of the outer segment of the margin based on a set of 25,000 km of multichannel seismic data acquired by the German Geological Survey (BGR). These data show that the margin structure and especially the SDRs vary in architecture, extent, and thickness along the margin. Franke et al. (2007) suggest that the location of the SDRs from 60 to 120 km wide was probably episodic, and the spread to the northern areas of the South Atlantic rift is widely developed. The South Atlantic Ocean opening created a series of marine basins, which can be observed on the continental shelf. From North to South some of them are the Colorado (CB), the Valdés (VB), the Rawson (RB), and Argentina basin (AB) (Fig. 1).

One of the most distinctive geophysical features of rifted continental margins is the free-air gravity edge-effect anomaly, which has generally been interpreted as the result of the juxtaposition of thick continental and thin oceanic crusts. The study of rheology, sedimentation, magmatism, and heat diffusion phenomena, that modify the initial crust structure for a rift, can help to understand the distinctive characteristic of the free-air gravity edge-effect of these kinds of margins. A useful way to analyze this issue is through a Process-Oriented Gravity Modeling (POGM) (Watts and Fairhead 1999; Watts 2001a, b; Pedraza De Marchi 2015; Pedraza De Marchi et al. 2017), where each geologic process is associated to a gravity anomaly. This modeling allows the possibility of isolating the effect of these geological processes involved in the evolution of the continental margin as they can be thought as independent events. Hence, the anomalies are called the rift anomaly, the sedimentation anomaly, and the magmatic underplating anomaly. POGM is based on potential-field data, whose results present an inherent ambiguity. However, POGM has reduced this ambiguity since it theoretically takes to account plausible schemes for the way how the sediment and magmatism load the crust flexurally (Watts and Fairhead 1999; Watts 2018), where the Airy case is implicit when the elastic thickness (Te) is 0 km.

In simple terms, the gravity anomaly as a signature of passive margins is composed of a "high" related to the continental shelf and a "low" associated with the slope region. This anomaly could be explained by a model in which the continent-ocean transition is located in the region of the present-day shelf break. However, the edge-effect is very sensitive to the location of the transition, changing abruptly if it is displaced a few tens of km landward or seaward of the shelf break (Watts and Fairhead 1999).
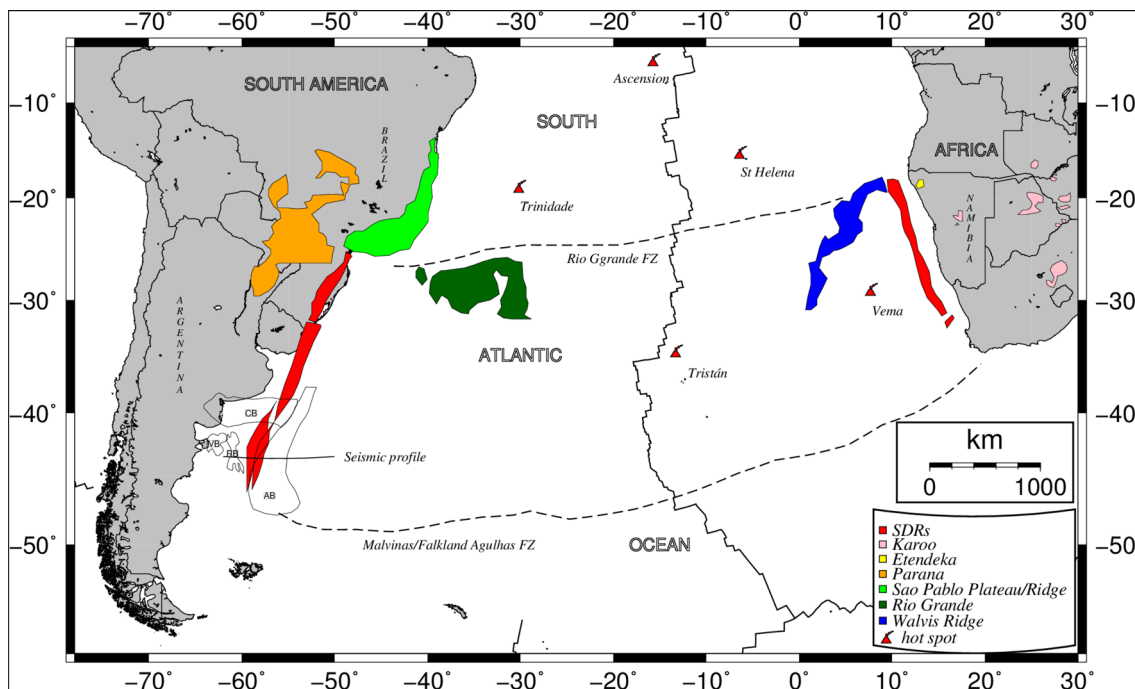
Fig. 1 Volcanic provinces of the conjugate parts of southern South Atlantic. Distribution of SDRs along the volcanic continental margin of South Africa and South America, Karoo, Etendeka, and Paraná continental flood basalts (CFB) as well as anomalous oceanic crustal regions (Sao Pablo Plateau/Ridge, Rio Grande, and Walvis Ridge related to Tristán Da Cunha hot spot (Tristan) in the South Atlantic. Furthermore, the Rio Grande and the Malvinas/Falkland Agulhas fracture zones connect the Cape and the Argentine basins (dotted black lines). Colorado (CB), Valdes (VB), Rawson (RB), and Argentina basins (AB) are pointed out. Prominent hot-spots are shown. The digitalized seismic profile is shown at 43.5°. Based on Figure 2.2 (Shuman 2002)

Margins in the South Atlantic region show a rather complicated gravity distribution due to mass inhomogeneities in the crust and upper mantle, which are the results of the long-lasting history of the breakup of the Gondwana supercontinent (Götze and Pail 2017).

We have modeled the magmatic underplating effect using POGM instead of conventional "static" modeling. In static modeling, the density structure is what best explains the gravity anomaly. This approach has been useful in determining the physical properties of the crust and mantle in continental margins. However, POGM is an innovative modeling that can distinguish the contribution that different geological processes provide to the observed gravity.

This work focuses on the estimation of the effect of magmatic underplating in the typical gravimetric edge-effect of rifted margins and the calculation of the flexural uplift associated with magmatic underplating in the Argentine continental margin.

Geological framework

The eastern continental margin of South America and the western continental margin of Africa are regions where a correlation between the continental break-up and associated magmatic events can be observed, resulting in large igneous provinces. The evolution of the Parana and Etendeka LIPs are commonly referred to the tectono-magmatic activities associated with Tristan da Cunha hot-spot (see Fig. 1) and its plume tail as the Walvis Ridge and the Rio Grand Rise (Morgan 1971; Wilson 1963). The Tristan da Cunha hot-spot could have triggered the opening of the South Atlantic Ocean (Richards 1989; Franke 2013).

The break-up of Gondwana supercontinent at around 155 Ma resulted in the formation of the South Atlantic continental margins (Ghidella et al. 2007; Jokat et al. 2003). Other studies (Gladczenko et al. 1997; Jokat et al. 2003; Nürnberg and Müller 1991; Rabinowitz and LaBrecque 1979) suggested that the breakup and subsequent opening of the oceans occurred earlier, between 137 and 126 Ma. Rabinowitz and Labrecque (1979) proposed that the opening occurred diachronically, rejuvenating from south to north.

The opening of the ocean basin was associated with the emplacement of large volumes of effusive volcanic rocks on Mesozoic intracratonic basins onshore and on the incipient rifted crust onshore and offshore (Bauer et al. 2000; Franke et al. 2007, 2010; Franke 2013; Gladczenko et al. 1997; Hinz et al. 1999; Jackson et al. 2000). Continental breakup and initial seafloor spreading in the South Atlantic Ocean were accompanied by extensive

transient magmatism as inferred from sill intrusions, flood basalt sequences, voluminous volcanic wedges, and high-velocity lower crust at the present continental margins. In seismic reflection data, voluminous extrusives are manifested by huge wedges of SDRs on the conjugate margins across the southern South Atlantic (Bauer et al. 2000; Blaich et al. 2011; Fernández et al. 2010; Franke et al. 2007, 2010; Gladczenko et al. 1997, 1998; Hinz et al. 1999; Jackson et al. 2000; Talwani and Abreu 2000). The extrusives lavas at the continental-ocean transition zone are underlain by a high seismic velocity (7.2–7.4 km/s), which is associated with voluminous igneous rocks intruded into the lower crust (Franke et al. 2010). Industry drilling off Namibia (Kudu Field) showed that the lavas were erupted sub-aerially (Clemson et al. 1999). The SDRs are emplaced symmetrically along the conjugate continental margins (Blaich et al. 2009; Talwani and Abreu 2000). High-velocity lower crust was identified by seismic studies in this segment of the South Atlantic (Bauer et al. 2000; Franke et al. 2006; Hirsch et al. 2009; Schnabel et al. 2008; Eldholm et al. 2000), with some indications that the volumes are more prominent at the eastern continental margin of South America than the western margin (Franke 2013).

A distinctive magnetic anomaly called G anomaly, described by Rabinowitz and Labrecque (1979) is mainly correlated with the (inner) wedges of SDRs (Bauer et al. 2000), signaling thick basaltic extrusives as the anomaly source. Underlying magmatic high velocity, a high-density body (7 km/s, 3000 kg/m^3) is reported from both sides of the South Atlantic (Gladczenko et al. 1997; Bauer et al. 2000; Franke et al. 2001). A seismic analysis performed along the Argentine margin by Blaich et al. (2009) indicates a high-density (3000 kg/m^3) intrusive body located below the syn-rift volcanic wedges (SDRs). High-density intrusive bodies within the rift are interpreted as mafic intrusions, originated by adiabatic decompression melting of the upper mantle (Cornwell et al. 2006). In this setting, the intrusive volcanic bodies within the mid-crust appear to be feeder dykes related to the emplacement of the SDRs and are probably connected to a magma reservoir located deeper in the crust. The magmatism along the Argentine margin is concentrated in a narrow zone within a broader zone of tectonic extension. This configuration suggests that the steady supply of magma through dykes may release stress, allowing the strain to occur at lower stresses than required for faulting. For this reason, the extension of the crust caused by magmatic intrusion exceeds the extension caused by tectonic strain (Ebinger and Casey 2001; Cornwell et al. 2006).

Data used

The data sources used in this work are free-air gravity anomaly, bathymetry, sedimentary thickness and a refraction profile.

Free-air gravity anomaly and bathymetry

The geoid is an equipotential surface of the terrestrial gravity field (without taking into account the effect of waves, winds, tides, and currents). Small elevations and depressions of the geoid (geoid undulations) can be measured using very precise radars aboard satellites (Sandwell and Smith 1997). A computationally demanding method for converting measurements of geoid elevation (with a variety of different accuracies, spacing paths, and data densities) into gravity anomaly grids (or images) have been developed by Sandwell and Smith (1997). The free anomaly grid of the V18.1 version of the Sandwell and Smith was used in this study. A comparison between marine gravity from ship and this version of satellite data can be seen in Pedraza De Marchi et al. (2012).

The bathymetry data belongs to the V14.1 version (Sandwell et al. 2001) and is constructed from a combination of different sources, such as marine gravity data derived from the Geosat and ERS-1 satellites with a horizontal resolution of 1–12 km.

Sedimentary thickness

A grid of sedimentary thicknesses has been performed using data from several sources and scanned results from published maps (e.g., http://www.martagh.com.ar/mararg/pictr 2002/). The data sources are: in marine zones from Ludwig et al. (1978) and in the terrestrial zones values from the figures of Zambrano and Urien (1970), a compilation of geological maps of the Argentine Republic (Caminos and González 1996) taken by the Naval Hydrographic Service (Parker et al. 1996) and Figure 5 of Neben et al. (2002). The data from this Figure are in two-way time (TWT) of the seismic signal in milliseconds, between the seabed and the breakup unconformity or basement. If the average sound velocity of 2000 m/s is assumed as an approximate estimate of the thickness, similar to Hayes and LaBrecque (1991), a maximum sedimentary thickness of 4000 m is obtained. The equation that relates to sedimentary thickness and single transit time (Coscia 2000) was applied. This is a semi-empirical law arising from the analysis of hundreds of solutions of the sedimentary layers at variable depths in different areas of the Argentine continental margin and was employed to calculate sedimentary thicknesses (Pedraza De Marchi et al. 2017). The sedimentary thickness along the 43.5°S profile was determined by interpolation in the grid.

Refraction profile

In 1998 and 1999, the Federal Institute for Geosciences and Natural Resources (BGR, Germany) acquired a seismic data set at the Argentine continental margin, including 12,000 km multichannel seismic (MCS) data and two wide-angle refraction seismic lines. One of the lines runs in the E–W direction at 43.5°S across the continental margin (Franke et al. 2002) (See Fig. 1). Franke et al. (2002) concluded that the Argentine continental margin velocity-depth model shows high similarity to the conjugated Namibian margin model (Bauer et al. 2000) with the implication of underplating (7.5 km/s layer) in both margins. The underplated layer is situated beneath the seaward dipping reflectors (SDRs), where a highly thinned crust was determined. Besides, by observations of reflector curvature, reflector length/continuity, and velocities in the wide-angle seismic data, they inferred that the formation of the dipping layers along the volcanic margin of the South Atlantic was episodic. The geometry of the magmatic underplated body used in our work is provided by the digitalization of the model across the margin (Figure 2 from Franke et al. 2002; see the interfaces in Fig. 6).

Fig. 2 Diagram for implementing the POGM method, TTS is total tectonic subsidence, β is the stretching factor and RMS is the root mean square. The highlight box is the step that this work emphasizes but all previous steps are necessary to arrive at this step. Based on Figure 6 Stewart et al. (2000)

Process-Oriented Gravity Modeling (POGM) method

The methodology of the POGM (Watts and Fairhead 1999; Watts 2001a, b; Stewart et al. 2000) technique can be described by the sequence of four steps, depicted in Fig. 2:
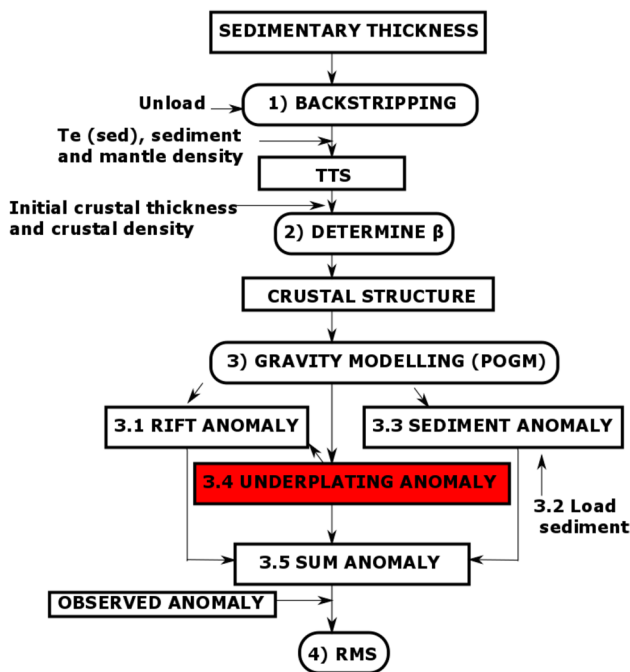
(1) Backstripping. This is a quantitative technique based on the removal of loads from the basement to obtain the total tectonic subsidence (TTS) (Watts and Ryan 1976). Backstripping can be calculated assuming that the load is locally (Airy) or regionally (Flexural) supported (e.g. Watts 1988). In this work and the overall POGM applications (Stewart et al. 2000; Watts 1988), TTS corresponds to the position of the basement in the absence of surface loads (such as sedimentary and volcanic) and subsurface loads (e.g. underplating).

In this study, backstripping is calculated by only one layer of sediment of average density, which is a simplification due to the sediment data are a combination of digitalization of geological charts and conversion of velocity models ("Sedimentary thickness" section), and we have no information from well data. Porosity value used was 0. In other words, we have not taken into account the effect of compaction.

Disregarding effects of the water loading due to changes in sea level, the tectonic subsidence/uplift y associated with a sediment thickness S^* is given by (Watts 2001a):

$$\widehat{Y}(k) = \widehat{S^*}(k)\phi(k)\left[\frac{\rho_s - \rho_w}{\rho_m - \rho_{infill}}\right], \tag{1}$$

where the hat in letters represents a 1D or 2D Fourier transform and k stands for the number of the linear or radial wave; ρ_m, ρ_w, ρ_s are the densities of the mantle,

Table 1 Parameters used in flexural and gravity modeling

Parameter	Symbol	Value
Density of seawater	ρ_w	1030 kg/m^3
Density of sediment layer	ρ_s	[1900–2700] kg/m^3
Density of crust	ρ_c	[2700–2800] kg/m^3
Density of mantle	ρ_m	3330 kg/m^3
Density of magmatic underplating	ρ_x	[2800–3300] kg/m^3
Density of asthenosphere	ρ_a	3260 kg/m^3
Thickness of zero elevation continental crust	T_0	32 km
Elastic thickness	T_e	[0–50] km
Average acceleration of gravity	g	9.81 m/s^2
Young's modulus	E	100 Gpa
Poisson's ratio	υ	0.25

water and the average of the sediment, respectively (Table 1), and $\phi(k)$, the waver parameter, is given by:

$$\phi(k) = \left[1 + \frac{Dk^4}{(\rho_m - \rho_{infill})g} \right]^{-1}, \qquad (2)$$

where g is the average acceleration of gravity and D is the flexural rigidity determined (Nm) from the effective elastic thickness T_e, which is a measure of the resistance to deformation of the lithosphere and is given by:

$$D = \frac{ET_e^3}{12(1 - v^2)}, \qquad (3)$$

where E is Young's modulus and υ Poisson's radius, which have standard values on continental margins (Table 1) (e.g. Watts and Stewart 1998; Stewart et al. 2000; Watts and Ryan 1976).

Considering the infill density (ρ_{infill}) as the water density rather than the sediment density, indicating that the vacant space is filled with water in the flexural unload. Flexural backstripping amounts to first computing the flexure due to the total sediment load with $\rho_{infill} = \rho_w$ and then subtracting the resulting flexure, w, from the observed thickness S*. Finally, backstriping can be calculated with:

$$h(x) = S^*(x) - y(x). \qquad (4)$$

In practice, a layer-by-layer flexural backstripping is carried out by assigning a different density and T_e. The flexural backstrip for a particular time is obtained by summing the loading effects of each layer, beginning for the first layer (Watts 2001a).

Then, the TTS is obtained by adding the present-day water depth (that is, the unfilled part of the basin) to the cumulative backstrip. This is the final depth the basin would have subsided to in the absence of sediment loading (Stewart et al. 2000).

(2) Determine the stretching factor (β): when TTS is known, we can derive the geometry of the rift based on the assumption that the thickness of the crust is locally compensated. Isostatic equilibrium according to Airy with a thickness crust prior to rifting is applied to calculate β. The β parameter is defined as the quotient between the unstretched and thinned crust. This parameter allows us to find the crustal structure and, therefore, the Moho topography at the time of rifting.

$$\beta = \left[\frac{T_c(\rho_m - \rho_c)}{T_c(\rho_m - \rho_c) - TTS(\rho_m - \rho_w)} \right], \qquad (5)$$

where T_c is a thickness crust, *TTS* is calculated for each T_e; ρ_m, ρ_c and ρ_w are the densities of the mantle, crust and water, respectively.

The Airy case is applied to obtain the stretching factor β. There are thermal arguments to justify the use of this model in this stage. Watts (2001a) shows in Figure 7.22 the relationship between the amount of stretching and crustal thickness and the magnitude of the sediment-derived backstrip and thickness. From this Figure, it can be concluded that the Airy model is a good approximation to McKenzie's model (McKenzie 1978). This is because thermal effects are important early and on so it is necessary when backstripping considers the changing density of the cooling crust and upper mantle (Watts 2001a).

(3) Gravity modeling: By calculating the gravity anomaly caused by the initial structure of the rift and due to the sedimentation and underplating processes and comparing it with the observed anomaly, a procedure that can restrict the *Te* values is obtained. Watts and Fairhead (1999) suggested calling this procedure "process-oriented gravity modeling" (POGM). POGM means to calculate the gravity anomaly caused by the initial structure of the rift and the associated anomaly with the modified processes. Then, comparing it with the observed anomaly, we obtain a procedure that can constrain the *Te* values by the following:

(3.1) The gravity anomaly due to backstripping obtained from a water-filled basin (water–crust interface) and its compensation (mantle–crust interface) is calculated. This is called the rift anomaly.

(3.2) The load of the sediment is given by the difference between the backstripping result and the current topography.

(3.3) The gravity anomaly due to sediment loading is obtained, and its compensation is calculated. This is known as the sediment anomaly.

(3.4) The gravity anomaly due to the underplating anomaly is obtained. This step is omitted for the crustal segments, which show no indication of magmatic underplating.

(3.5) In the final step, the sum anomaly due to the rift, sedimentation, and underplating is calculated.

(4) Sum anomaly. The sum anomaly and the observed anomaly on the rift basin are compared through the root mean square (RMS) calculated by the difference between observed and calculated anomaly.
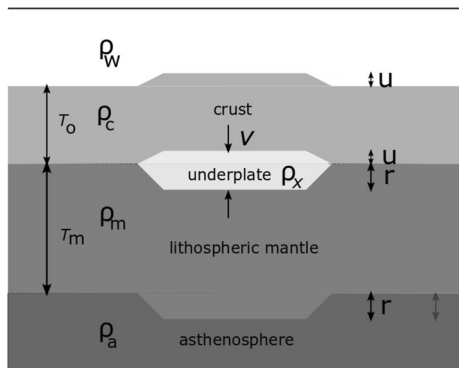
Fig. 3 Simple model of magmatic underplating of a crust of uniform thickness. Based on Figure 7.26 Watts (2001a)

Simple model of magmatic underplating

Magmatic underplating disturbs the isostatic state of a region. Consequently, we can estimate the amount of uplift (McKenzie 1984; Watts 2001a) that would result by balancing a column of crust that has been underplated with one that has not (Fig. 3) as follows in the equation:

$$u\rho_w + T_o\rho_c + T_m\rho_m + r\rho_a = T_o\rho_c + v\rho_x + T_m\rho_m, \quad (6)$$

where u is the amount of uplift, v is the thickness of the magmatic underplated material, $r = v - u$, $\rho_w, \rho_c, \rho_m, \rho_a$ and ρ_x are the densities of the water, crust, mantle, asthenosphere and underplated material, respectively. T_o is the crustal thickness, and T_m is the thickness of the lithospheric mantle (see Fig. 3).

$$\therefore u\rho_w + \rho_a r = v\rho_x \quad (7)$$

$$u\rho_w + \rho_a(v - u) = v\rho_x \quad (8)$$

$$\therefore u = v\frac{(\rho_a - \rho_x)}{(\rho_a - \rho_w)}. \quad (9)$$

Watts (2001a) provides an example for an underplated body at Hatton Bank (Fowler et al. 1989) wherein he used $v = 15$ km, $\rho_a = 3200$ kg m^{-3}, $\rho_w = 1030$ kg m^{-3}, and $\rho_x = 2900$ kg m^{-3}, (in the Eq. 9) obtaining u = 2.41 km.

In order to calculate the flexural effects, the appropriate wave parameter (Φ_e) that modifies the Airy response (Eq. 9) to the one that produces the flexure is defined by:

$$U(k) = V(k)\frac{(\rho_a - \rho_x)}{(\rho_a - \rho_w)}\phi_e(k), \quad (10)$$

where U(k) and V(k) are the Fourier transform of the uplift and the thickness of the underplating, respectively, and Φe

is the parameter in the wavenumber domain as in the following equation:

$$\phi_e(k) = \left[1 + \frac{Dk^4}{(\rho_a - \rho_w)g}\right]^{-1}, \quad (11)$$

where g is the average acceleration of gravity, this value is not very significant in this calculation, therefore the standard value g = 9.81 m/s^2 is used (Table 1), and D is the flexural rigidity determined (Nm) from the effective elastic thickness T_e.

Recognition of the synthetic anomalies derived by POGM

Figure 4 shows synthetic gravity anomalies for simple models, which have been calculated using POGM. As it was described in "Process-Oriented Gravity Modeling (POGM) method" section, POGM consists of a series of steps: (1) Backstriping to determine the TTS considering flexure (dashed line in 4d, 4g, and 4i in Fig. 4); Calculating the amount of flexural uplift that allows finding the corresponding interfaces to be used in the calculation of underplating anomaly, (2) Obtaining β, and recovering the geometry of the Moho at the time of rifting (i.e. the backstripped Moho) assuming an Airy model of rifting, and (3.1) computing the rift anomaly (water–crust + mantle–crust). This resulting anomaly shows the characteristic edge-effect of passive margins (4a in Fig. 4), (3.2) Restoring the sediment load to the margin and computing the flexure for the Te structure were performed in step 1. (3.3) The gravity anomaly associated with the sedimentation processes (without magmatic underplating) can be obtained by adding the loading (sediment–water) and the flexural effects (sediment–crust + crust–mantle interfaces) (4f in Fig. 4. The gravity anomaly associated with the underplating processes can be obtained by adding the effects of (water–crust + crust–underplating + mantle–underplating + asthenosphere–mantle interfaces) (4c in Fig. 4) (see "Simple model of magmatic underplating" section), (3.5) Adding the rift and underplating anomaly (4e in Fig. 4) or the rift and sedimentation anomaly (4h in Fig. 4), and (4) comparing the sum to the observed gravity by varying the Te structure used in the backstripping, different sum anomalies will be computed, and constraints will be able to be placed on the long-term mechanical structure across the margin section. Additional constraints can be obtained by comparing the final geometry of the gravity Moho (i.e. the flexed Moho in 4d or 4g in Fig. 4) to the seismic Moho constrained from data (Cunha 2008) (Fig. 8). In the following section, we explain how to obtain the sum anomaly where there is
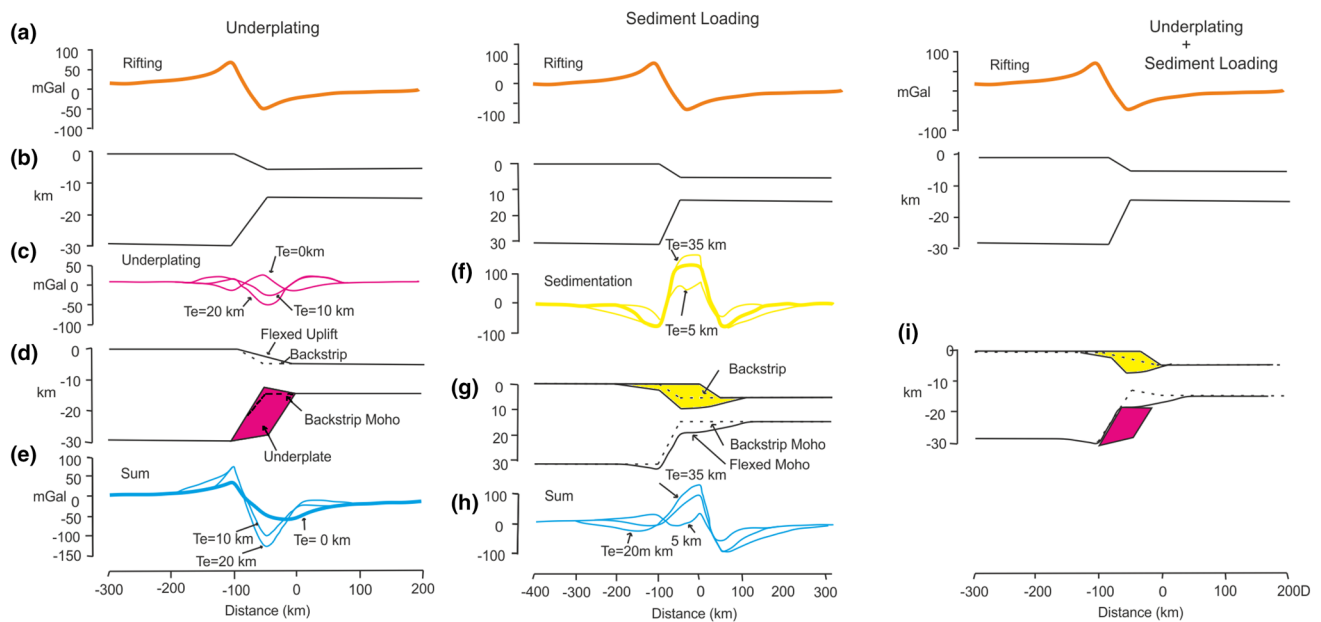
Fig. 4 Gravity anomalies associated with **a** rifting, **c** underplating and **f** sedimentation. Loading of **d** underplating, **g** sedimentation, and **i** underplating and sedimentation. Structure of the crust associated with rifting **b**. Influence of the underplating anomaly on the sum anomaly (rift and underplating anomaly) for values of elastic thickness 0, 10 and 20 km **e**. Influence of the sedimentation anomaly on the sum anomaly (rift and sedimentation anomaly) for values of elastic thickness 5, 20 and 35 km **h**. Modified from Figures 2 and 3 (Watts and Fairhead 1999)

a combination of the sedimentation and underplating processes (corresponding geometry in 4i in Fig. 4).

Scheme to calculate the sum anomaly with the combination of magmatic underplating and sediment loading

Figure 5 shows a simple synthetic scheme to understand the interfaces involved in the calculation of the gravity anomalies. In this work, we used the flexural model to model sediment and underplating loadings, as we mentioned before, the Airy case is an extreme case. For simplicity, the scheme looks like the Airy case and only should be observed to analyze the interfaces involved in each contribution. In Fig. 5a, the bathymetry (1) and lithospheric mantle (2) interfaces are used to calculate the rift anomaly; in Fig. 5b the (3), (4), and (5) interfaces are used to calculate the sediment anomaly without taking into account the magmatic underplating; in Fig. 5c the (3), (4), (5) and (6) interfaces are used to calculate the magmatic underplating anomaly; and in Fig. 5d the (7), (8), (9) and (10) interfaces are used to calculate the sedimentation anomaly considering magmatic underplating.

Results and discussion

The flexure calculations using POGM assume a simple elastic plate model and uniform density for water, sediment, crust, underplating, and mantle. In the profile at the 43.5°S of the Argentine continental margin between 62°W and 50°W, models with different densities of the underplated body, crust, and sediment were used to test POGM (called POGM models). All POGM models have been tested for standard values of mantle ($\rho_m = 3330$ kg/m^3) and asthenosphere density ($\rho_a = 3260$ kg/m^3), for a range of sediment ($\rho_s = [1900$ kg/m^3–2700 kg/m^3]), for a range of underplated body ($\rho_x = [2850$ kg/m^3–3300 kg/m^3]) and crustal densities ($\rho_c = [2700$ kg/m^3–2800 kg/m^3]) (Table 1). A total of 45 POGM models were obtained, of which four models have been selected with RMS < 5 (see Table 2). The RMS is calculated only in the area of magmatic underplating, which is for the distance from the point (43.5S, 62W) between 200 and 500 km. The incorporation of the magmatic underplating effect in POGM increases the elastic thickness of the RMS minimum (see Table 2). This result is due to the fact that the crust became thicker with the magmatic underplating (Watts 2001a, b; Watts et al. 2009) and a model with a strong margin can explain it better. The RMS of gravity strongly decreased (b, in Table 2) when POGM includes the magmatic underplating. The RMS is 4.82 on average in this
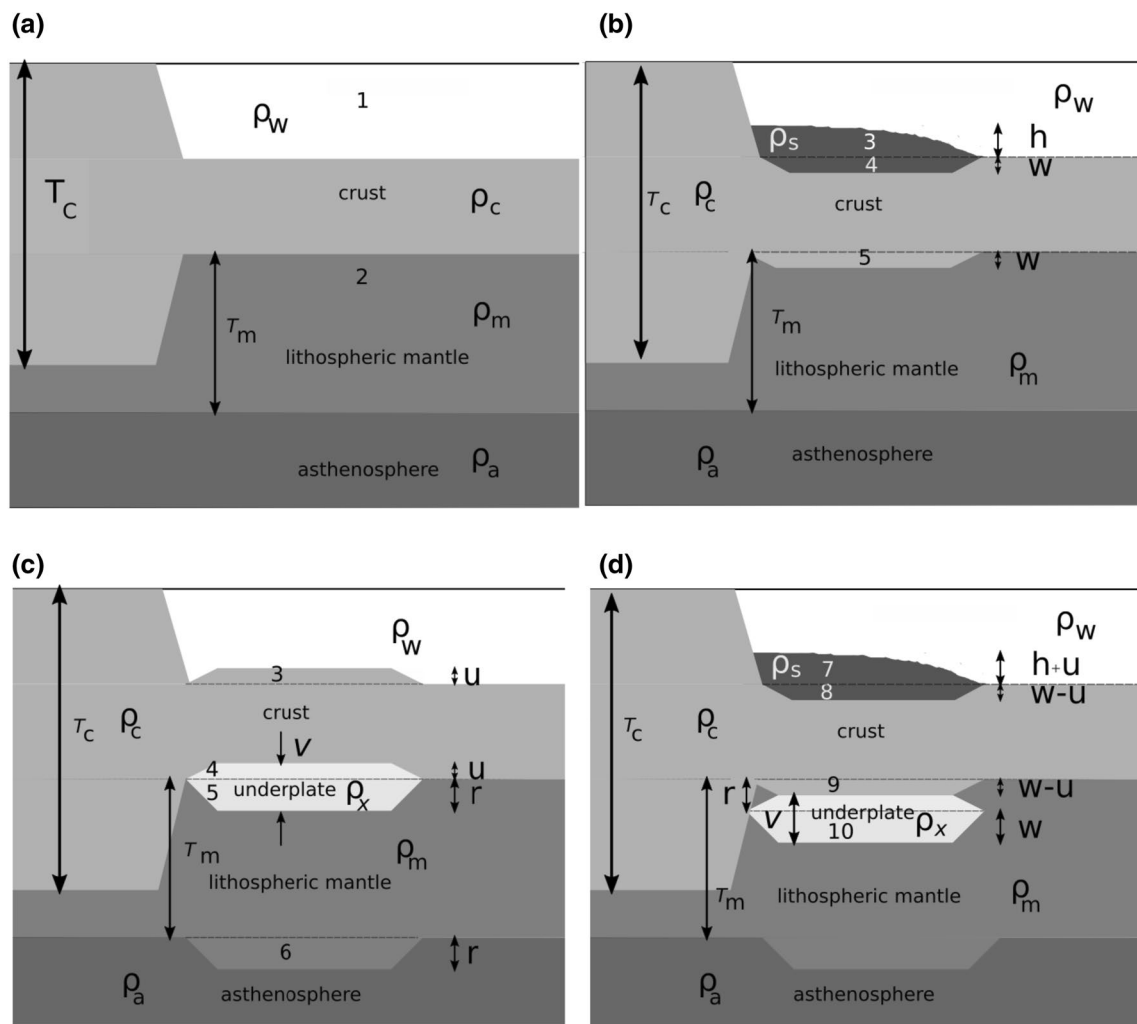
Fig. 5 A simple POGM scheme showing interfaces with and without magmatic underplating. **a** The rift interfaces, **b** the sediment interfaces without magmatic underplating; **c** the magmatic underplating interfaces, and **d** the sedimentation interfaces with magmatic underplating

Table 2 Minimum RMS of gravity for different densities and elastic thicknesses: (a) without considering the magmatic underplating, (b) taking into account the magmatic underplating

	a, b	a, b	a	a	b	b	b	b
	ρ_c [kg/m³]	ρ_s [kg/m³]	RMS of gravity	Te [km]	ρ_x [kg/m³]	RMS of gravity	Te [km]	um [m]
Model 1	2750	2200	9.12	25	3125	4.57	35	147.88
Model 2	2775	2250	9.17	20	3150	4.76	30	131.56
Model 3	2750	2150	9.04	25	3125	4.79	35	147.88
Model 4	2800	2300	8.93	20	3150	4.88	30	131.56

um is the maximum flexural uplift value along the profile

Table 3 Statistical parameters: mean and standard deviation (SD) for 45 POGM models with RMS < 5

|	a,b	a,b	a	a	b	b	b	b
	ρc [kg/m³]	ρs [kg/m³]	RMS of gravity	Te [km]	ρx [kg/m³]	RMS of gravity	Te [km]	um [m]
Mean	2755	2207.78	9.15	24	3133.89	4.82	33.89	140.32
SD	35.59	42.58	0.24	2.02	22.71	0.09	2.36	22.12

case and 9.15 on average when the effect is not considered (Table 3).

Since POGM is based on the potential field methods, the results have an inherent ambiguity. For this reason, Table 3 (keeping the references for a and b from Table 2) provides the mean and standard deviation of the 45 models given in Table 2. The resulting average density of magmatic underplating ($\rho_x = 3133.89$ kg/m$^3 \pm 22.71$ kg/m^3) is close to the average between the densities of crust and mantle. According to Schnabel et al. (2008), the ρ_x parameter in the same digitalized refraction profile in this paper is 3150 kg/m^3. The average sediment density value ($\rho_s = 2207.78$ kg/m$^3 \pm 42.58$ kg/m^3) is included in the interpreted density range (1700–2400 kg/m^3) by the same author for at least two sediment layers. Average elastic thickness values $T_e = 24$ km ± 2.02 km without magmatic underplating and $T_e = 33.89$ km ± 2.36 km with it were used in final models in Fig. 9. The latter T_e is in the range of values that can be observed in Figure 7 of Pérez-Gussinyé et al. (2007) in the marine area. Finally, the average flexural uplift resulted in the Argentine margin is um $= 140.32$ m ± 22.12 m, which is relatively smaller than the estimated uplift in the Hutton bank (um $= 2.41$ km) due to the possibility that the density of the assumed underplated body is close to the asthenosphere density and that imposes a bias in the underplating equation (Eq. 10). According to Maclennan and Lovell (2002), the uplift produced by magmatic underplating may contribute an amount equal to $\sim 10\%$ of the thickness of the underplated body. The thickness of the underplated body is on average 3 km, and our calculated uplift is $\sim 5\%$ of this value.

We tested the effect of crustal density variations in Moho depth undulations by comparing the POGM Moho result with seismic Moho. We find that the obtained Moho boundary is shallower than the seismic Moho for $\rho_c = 2700$ kg/m^3 (Fig. 6a) and relatively deeper for $\rho_c = 2800$ kg/m^3 (Fig. 6c). We considered a tradeoff density value of $\rho_c = 2755$ kg/m^3 for the computation, which is from the estimation in Table 3 and visual inspection in Fig. 6b.
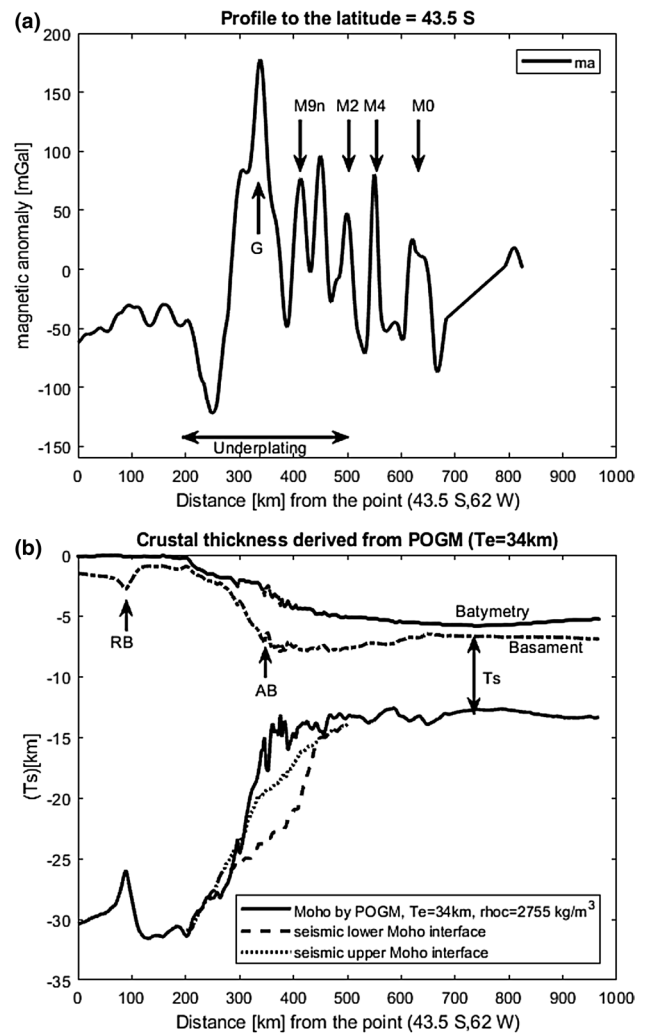
Fig. 7 a Magnetic anomaly profile from grid performer by Ghidella et al. (2006). G anomaly is from Rabinowitz and Labrecque (1979), and M series are from Ghidella et al. (2006, 2007), and **b** crustal thickness derived from POGM (Ts) ($T_e = 34$ km and an average crustal density of $\rho_c = 2755$ kg/m^3). The location of Rawson (RB) and Argentina basin (AB) are pointed out
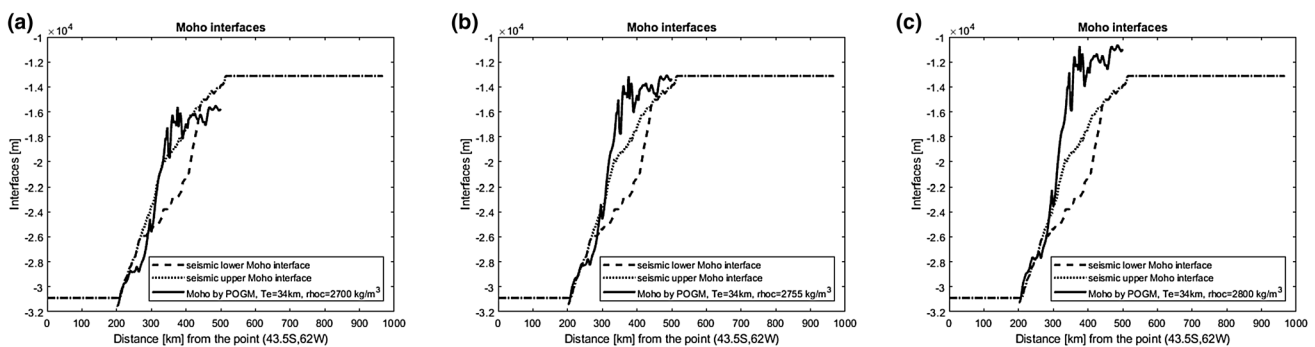

Fig. 6 Moho interfaces derived from POGM calculation vs seismic Moho (Franke et al. 2007) for **a** $\rho_c = 2700$ kg/m^3, **b** an average crust density of $\rho_c = 2755$ kg/m^3, and **c** $\rho_c = 2800$ kg/m^3

Figure 6 shows the Moho interfaces where the thick dashed line corresponds to the modeled Moho by using POGM, and the continuous line and dot-dashed line are the digitalized interfaces from the seismic profile at 43.5°S ("Refraction profile" section), which we have called seismic lower Moho interface (below the underplated body) and seismic upper Moho interface (above the underplated body), respectively. The comparison between seismic Moho and Moho by POGM reveals that the latter is considerably similar to the one obtained with seismic results for case (b), which is re-plotted in Fig. 7b.

Figure 7 shows the magnetic anomaly along the profile where the prominent positive linear magnetic G anomaly is marked (it was identified by Rabinowitz and LaBrecque (1979) and published later by Hinz et al. (1988), marks the boundary between continental and oceanic crust) and the M series, particularly the positive M0, M9n, M2, and M4 anomalies following Ghidella et al. (2006, 2017) (a) and the crustal thickness derivated from POGM calculations (Ts) (it is characterized by a thinned crust in the ocean area and a strong gradient near to the underplated body) (b). We can estimate the oceanic crustal thickness, which is Ts = 6.36 km on average.

Figure 8 shows the rifting, sedimentation, and underplating anomalies of POGM. The rifting anomaly is characterized by two edge-effects, one corresponding to the Rawson basin region and the other to the self break position in the Argentine basin region (Fig. 8a). The sedimentation anomaly is characterized by two "highs" linked with the Rawson basin and the Argentine basin (a central "high", which is flanked by two "lows"). The "high" arises because sediments are denser than the water that they displace while the "low" is the result of the downward displacement of the relatively low-density sediment into the crust and relatively low-density crust into the mantle by the sediment load (Fig. 8b) (Watts 2001a, b). Finally, the underplating anomaly appears in Fig. 8c. Magmatic underplating implies a re-distribution of mass that should be associated with the gravity anomalies (Watts 2001a). The gravity effect of magmatic underplating depends on two factors: the first one generates a "low" due to the low density of the underplated material and the other one a "high" due to the water displacement by the uplift of the crust. The associated anomaly is strongly dependent on the elastic thickness (Te) of the lithosphere. At a weak margin (Te = 0 km) the amplitude of the "high" and "low" effects are small and the wavelength is relatively long, while at a strong margin (Te = 20 km) the opposite effect occurs; the magmatic underplating increases the amplitude of the "high" and "low" effects and decreases its wavelength (Watts and Fairhead 1999). The magmatic underplating anomaly presents opposite contributions for the Airy and flexural cases, the amplitude is < 13 mGal in all curves
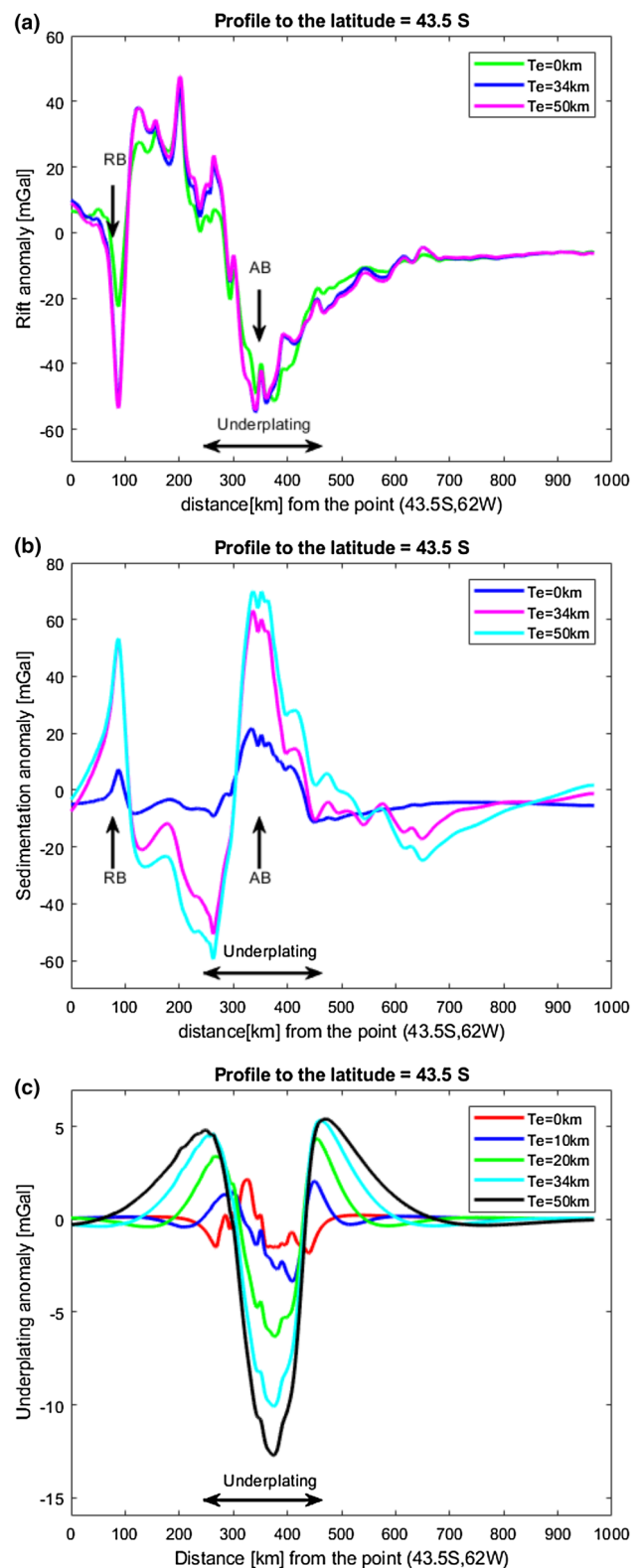
Fig. 8 Gravity anomalies derived from POGM: **a** rift anomaly, **b** sedimentation anomaly, **c** magmatic underplating anomaly calculated by $\rho_x = 3134$ kg/m^3. The location of Rawson (RB) and Argentina basin (AB) are pointed out in **a** and **b**

(a)

Profile to the latitude = 43.5 S

(b)

Profile to the latitude = 43.5 S
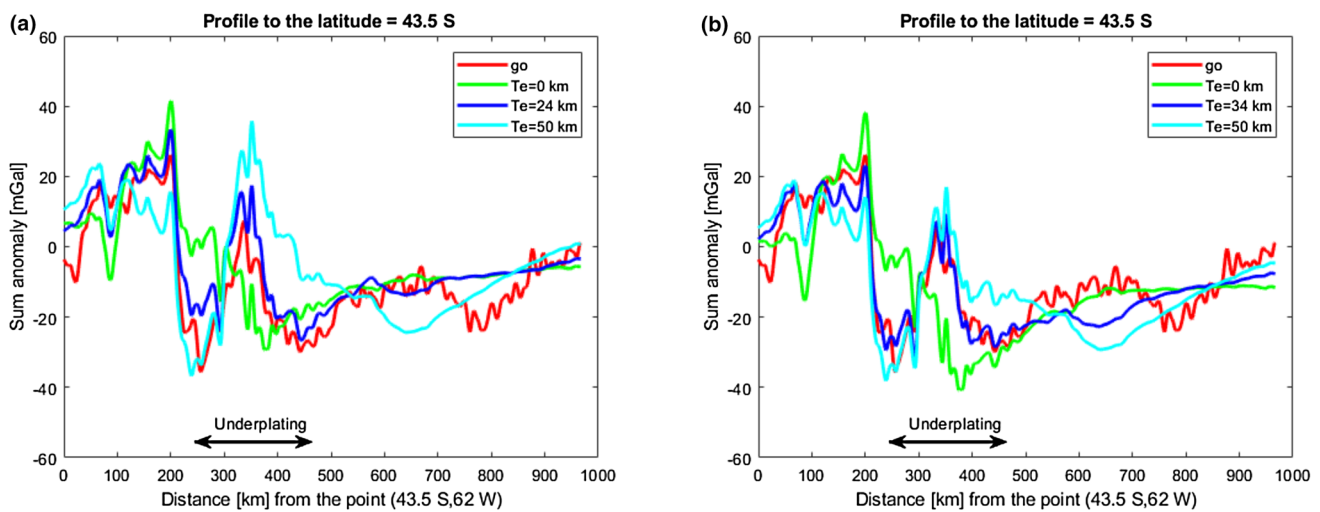
Fig. 9 Sum anomaly: **a** without taking into account magmatic underplating. **b** Taking into account magmatic underplating; go is the observed gravity, and the other curves were obtained by varying the

Te in the POGM (Te = 0 km corresponds to Airy, blue corresponds to Te = 24 km in **a** and Te = 34 km in **b**)

shown in Fig. 8c and its lateral lobes are asymmetric. This behaviour would respond to the geometry of the underplated body that is shallower at the east. In the case of Te = 34 km, the maximum underplating anomaly has an approximate value of − 10.10 mGal, which is not a negligible effect considering that is calculated from a body at an average depth of 20 km (Fig. 7b) and the contribution of the asthenosphere interface is approximately 2 mGal.

The calculated gravity signal (if Te is not zero), in the sector of magmatic underplating (Fig. 9a) has a "high" where the underplating anomaly (Fig. 8c) has a "low" and has two "lows" where the underplating anomaly has two "highs". Therefore, adding the underplating anomaly to the sum anomaly produces the best fit with the observed anomaly and an increase of the elastic thickness (Fig. 9) of the fit according to the fact that the underplating produces a thickening of the crust; this effect changes the amplitude of the calculated anomaly without substantially changing its form.

Figure 9 shows the calculated POGM gravity anomaly (sum anomaly) when the effect of magmatic underplating was not considered (Fig. 9a) and when it was (Fig. 9b). The curve for the average elastic thickness Te = 34 km follows the observed gravity more closely in Fig. 9b than in Fig. 9a with average elastic thickness Te = 24 km, especially in the underplating area, which shows that the best fit is achieved by incorporating magmatic underplating effect.

A continental margin is a complex area where oceanic and continental crust is joined. Characterizing the zone with only one value of Te is a first approximation to solve the current and old complex margin structure. Oceanic flexure studies suggest that Te is in the range of 2–40 km and that it depends on the load and the age of the plate. On the other

Profile to the latitude = 43.5 S
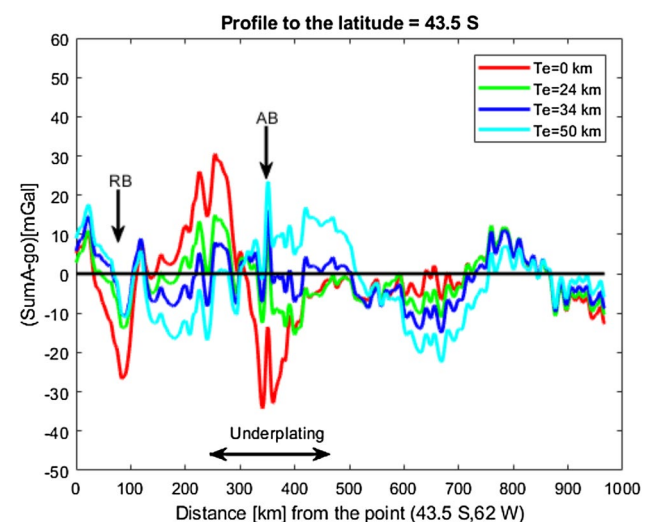
Fig. 10 Estimated isostatic anomaly considering underplating except for green curve, which is the case where it is not considered. The location of Rawson (RB) and Argentina basin (AB) are pointed out

hand, Te in the continents ranges from 0 to 100 km and shows no clear relationship with age (Burov and Watts 2006; Watts 2001b). In the oceans, Te is given approximately by the depth to the 450 °C isotherm in concordance with cooling plate models. For example, Te increases from 4 to 12 km at the mid-oceanic ridge where the lithosphere is relatively young and hot to values > 30 km where it is old and cold. However, studies in the continents do not show such a simple relationship between Te and thermal age (Watts and Fairhead 1999).

Passive margins are formed by horizontal extension of continental lithosphere that results in lithospheric thinning and subsequent subsidence or uplift, which occur to maintain the isostatic balance (Esedo et al. 2012). As a first approximation, the isostatic anomaly could be used to restrict the Te of mode-ling.

Figure 10 shows an estimation of isostatic anomaly calculated from the difference between sum anomaly from POGM and the observed gravity when the effect of magmatic underplating was not considered (case Te = 24 km in Fig. 9a) and when it was (all curves of Fig. 9b). The curve for the average elastic thickness Te = 34 km (blue curve) produces tiny variations around zero in the underplating area, which means that isostatic anomaly is minimum, and ideally, the isostatic balance is achieved in the area of the Argentine basin, but as we mentioned before, there is a mismatch in the oceanic crustal region beyond 500 km.

"Static" gravity models, called Object-Oriented Gravity Modeling (OOGM) by Watts (2018), are probably more common than POGM. According to Watts, OOGM and POGM are based on the density structure and yield the same results when they are compared. But in POGM, one or more geological processes, such as sediment loading considered, along with density, and parameters such as the flexural rigidity of the lithosphere are varied until a fit is obtained. The POGM models used in this paper are simple and only consider rifting, uniform (Airy-type) crustal thinning, and constant densities and loading. However, POGM can be modified to include non-uniform extension with depth (Royden and Keen 1980), strength during rifting (Watts and Stewart 1998), and variable density distribution in the sediment with depth (Granser 1987). POGM derived gravity anomalies yield information not only on the physical structure but also on geological processes in the past (Watts 2018). Although the time evolution of the properties and responses of the Earth during the involved geological processes is not within the scope of our work, we know that the properties of the lithosphere are heterogeneous in both space and time in the rift zone and the remaining continent-ocean lithospheric passive margin (thickness, flexural rigidity, etc.) and should be considered in more complex models. In Pedraza De Marchi et al. (2017), the POGM method is applied without taking into account the magmatic underplating in an extensive area of the Argentine continental margin. This regional study represents an important contribution to isostatic studies and the current knowledge of the structure of the crust of the region. The analysis of results included: the characterization of sedimentary basins by a thinned crustal thickness, which according to stretching factors could show stretching periods that did not reach the stage of oceanic crust formation; the location of a strong structural variation of crustal thickness, which could be associated with the COB (crust-oceanic-boundary); an alignment in rift anomaly of Valdés

and Rawson basin, which is continued on a possible third basin that could be an aborted rift or aulacogen. This can be seen on a crustal thickness map (Figure 7 in Pedraza De Marchi et al. 2017) as evidence of a cortical shortening; an estimation of the isostatic anomaly that showed a strong positive residue in the Colorado basin, which could suggest that the basin may continue in subsidence as pointed out by Introcaso (2003).

A passive margin is not a plate boundary, the South American plate is one rigid entity composed of a continental part and an oceanic part. To zero-order, one can pile up the gravitational effects of all the parts and get a reasonable final state, which is basically what one does in the OOGM models, which can also include flexure. In both classes of models (OOGM or POGM), it would be desirable that overall geometry comes from seismic data (reflection and refraction).

Figure 8c confirms that the anomaly associated with magmatic underplating has the opposite effect for the flexural and Airy cases and, as shown in Fig. 9b, the flexural magmatic anomaly for Te = 34 km produces the best-fitting sum anomaly. The Airy anomaly gives the worse fit since the sum anomaly does not follow the tendency of observed gravity. This result supports the idea that it is essential to consider the flexure in gravity modeling of a passive margin and that exploring POGM models can help us deal with this issue.

Conclusions

In this work, we assumed a simple forward model, POGM, in which the water-filled basin that forms as a result of rifting is compensated for an Airy model. The model makes the assumption that the lithosphere has not a flexural behavior during the rift. The amount of crustal thinning, the thickness of sediment, and underplating and Te are specified before calculating the gravity anomalies. We adopt "process-oriented" instead of "object-oriented" scheme because it has reduced the inherent ambiguity in the potential field data since it theoretically takes into account plausible schemes for understanding the effect of sediment and magmatic loads on the flexure of the lithosphere. This procedure implies backstripping and gravity anomalies.

(1) We estimated an average maximum flexural uplift associated with the magmatic underplating of $140.32 \text{ m} \pm 22.12$, which is ~ 5% the thickness of the underplated body, an average density of the underplated body of $\rho_x = 3133.89 \text{ kg/m}^3 \pm 22.71 \text{ kg/m}^3$, an average density of the sediment of $\rho_s = 2207.78 \text{ kg/m}^3 \pm 42.58 \text{ kg/m}^3$, and average density of crust of $\rho_c = 2755 \text{ kg/m}^3 \pm 35.59 \text{ kg/m}^3$. The underplating and sediment densities have been contrasted with those obtained by Schnabel et al. (2008). Surprisingly, the

amount of uplift is one order of magnitude less than the one calculated by Watts (2001a) in the Hatton Bank continental margin. This is due to the fact that the density of the underplated body is close to the asthenosphere density in the Argentine margin.

(2) All POGM models tested in this work lead to an increase in elastic thickness compared to the calculation that leaves out the magmatic underplating. However, a mismatch in the oceanic crustal region was observed since characterizing the zone with only one value of Te is a first approximation to solve the current and old complex margin structure.

(3) The resulting average elastic thickness from the POGM modeling is for a strong margin (Te = 34 km) and the estimated oceanic crustal thickness on average is Ts = 6.36 km.

(4) The magmatic underplating anomaly is characterized by two "highs" and a "low" wherein the sum anomaly (without the magmatic underplating) has two "lows" and a "high", respectively. The resulting amplitude of the anomaly is − 10.10 mGal.

(5) We verify that, in the Argentine margin, the underplating anomaly presents opposite contributions to the Airy and flexural cases as pointed out by Watts and Fairhead (1999) in their synthetic tests. This is one of the reasons why we consider that flexural models cannot be "ignored" in gravity anomalies interpretation on passive margins.

We need to include a more comprehensive analysis of geophysical and geological data to improve the knowledge of the rift-related processes that are linked with the underplating and thus to continue contributing to the understanding of the complex issue of Argentine margin evolution.

References

Bauer K, Neben S, Schreckenberger B, Emmermann R, Hinz K, Fechner N, Gohl K, Schulze A, Trumbull RB, Weber K (2000) Deep structure of the Namibia continental margin as derived from integrated geophysical studies. J Geophys Res 105:25829–25853

Beard J, Ragland C (2005) Reactive bulk assimilation: a model for crust-mantle mixing in silicic magmas. Geology 33(8):681–684. https://doi.org/10.1130/G21470AR.1

Blaich OA, Faleide JI, Tsikalas F, Franke D, Léon E (2009) Crustal-scale architecture and segmentation of the Argentine margin and its conjugate off South Africa. Geophys J Int 178:85–105

Blaich OA, Faleide JI, Tsikalas F (2011) Crustal breakup and continent-ocean transition at South Atlantic conjugate margins. J Geophys Res 116:B01402

Burov EB, Watts AB (2006) The long-term strength of continental lithosphere: "jelly sandwich" "crème brulée"? Gsa Today 16(1):4–10

Caminos R, González PD (1996) Mapa Geológico de la República Argentina. Servicio Geológico Minero Argentino (SEGEMAR), Buenos Aires, Argentina. https://repositorio.segemar.gov.ar/handle/308849217/1542

Coscia CA (2000) Aprovechamiento de los datos sísmicos preexistentes para el análisis del espesor sedimentario en el margen continental argentino. En: Seminario de la Plataforma Continental, Buenos Aires, publicación del Consejo Argentino para las Relaciones Internacionales (CARI), pp 249–265

Clemson J, Cartwright J, Swart J (1999) The Namib rift: a rift system of possible Karoo age, offshore Namibia. In: Cameron NR, Bate RH, Clure VS (eds) The oil and gas habitats of the South Atlantic. Geological Society, London, Special Publication, London, pp 381–402

Cornwell DG, McKenzie D, England RW, Maguire PKH, Asfaw LM, Oluma B (2006) Northern Main Ethiopian Rift crustal structure from new high-precision gravity data. Geol Soc Lond Spec Publ 259:307–321

Cox KG (1993) Continental magmatic underplating. Philos Trans R Soc 342(1663):155–166

Cunha T (2008) Gravity anomalies, flexure and the thermo-mecanical evolution of the West Iberia Margin and its Conjugate of Newfoundland. PhD Thesis, University of Oxford, Wolfson College & Department of Earth Sciences, p. 344

Ebinger CJ, Casey M (2001) Continental breakup in magmatic provinces: an Ethiopian example. Geology 29:527–530

Eldholm O, Gladczenko TP, Skogseid J, Planke S (2000) Atlantic volcanic margins: a comparative study. In: Nøttvedt A, Larsen BT, Olaussen S, Tørudbakken B, Skogseid J, Gabnelson RH, Brekke H, Birkeland O (eds) Dynamics of the Norwegian margin. Geological Society of London Special Publication 167. The Geological Society, London, pp 411–428

Esedo R, van Wijk J, Coblentz D, Meyer R (2012) Uplift prior continental breakup: indication form removal of mantle lithosphere? Geosphere 8:1078–1085

Fernández M, Afonso JC, Ranalli G (2010) The deep lithospheric structure of the Namibian volcanic margin. Tectonophysics 481:68–81

Fowler SR, White RS, Spence GD, Westbrook GK (1989) The Hatton Bank continental margin. 2. Deep-structure from 2-ship expanding spread seismic profiles. Geophys J R Astron Soc 96:295–309

Franke D (2013) Rifting, lithosphere breakup and volcanism: Comparison of magma-poor and volcanic rifted margins. Mar Pet Geol 43:43–67

Franke D, Hinz K, Oncken O (2001) The Laptev Sea rift. Mar Pet Geol 18:1083–1127

Franke D, Neben S, Hinz K, Meyer H, Schreckenberger B (2002) Hidrocarbon habitat of volcanic rifted passive margins. APGHedberg conference

Franke D, Neben S, Schreckenberger B, Schulze A, Stiller M, Krawczyk CM (2006) Crustal structure across the Colorado Basin, offshore Argentina. Geophys J Int 165:850–864

Franke D, Neben S, Ladage S, Schreckenberger B, Hinz K (2007) Margin segmentation and volcano-tectonic architecture along the volcanic margin off Argentina/Uruguay, South Atlantic. Mar Geol 244:46–67

Franke D, Ladage S, Schnabel M, Schreckenberger B, Reichert C, Hinz K, Paterlini M, de Abelleyra J, Siciliano M (2010) Birth of a volcanic margin off Argentina, South Atlantic. Geochem Geophys Geosyst 11:Q0AB04. https://doi.org/10.1029/2009GC002715

Ghidella ME, Schreckenberger B, Paterlini CM, Abraham DA (2006) Anomalías magnéticas en el margen argentino. Actas en CD-ROM de la XIIIa. Reunión de Tectónica (San Luis, 16–20 octubre 2006), 4 pp. ISBN 978-987-1031-49–8

Ghidella ME, Lawver LA, Gahagan LM (2007) Break-up of gondwana and opening of the south atlantic: review of existing plate tectonic models. U.S. Geological Survey and The National Academies; USGS OF-2007-1047, Short Research Paper 055. https://doi.org/10.3133/of2007-1047.srp055

Ghidella M, Pedraza De Marchi AC, Paterlini M, Abraham D (2017) Anomalías magnéticas en el margen argentino (MARARG), ISSN: 2007-9656-LatinMagLetters, Universidad Nacional autónoma de México. http://www.geofisica.unam.mx/LatinmagLetters/LL17-01-SP/LM17-0101SP.html

Gladczenko TP, Hinz K, Eldholm O, Meyer H, Neben S, Skogseid J (1997) South Atlantic volcanic margins. J Geol Soc 154:465–470

Gladczenko TP, Skogseid J, Eldhom O (1998) Namibia volcanic margin. Mar Geophys Res 20:313–341

Granser H (1987) Three-dimensional interpretation of gravity data from sedimentary basins using an exponential density-depth function. Geophys Prospect 35:1030–1041

Götze HJ, Pail R (2017) Insights from recent gravity satellite missions in the density structure of continental margins. With focus on the passive margins of the South Atlantic. Gondwana Res. https://doi.org/10.1016/j.gr.2017.04.015

Hayes DE, LaBrecque JL (1991) Sediment isopachs: circum-Antarctic to 30°S. In: Hayes DE (eds) Marine geological and geophysical atlas of the circum-antarctic to 30°S. Antarctic Research Series. AGU, Washington DC, USA

Hinz K (1981) A hypothesis on terrestrial catastrophes: wedges of very thick oceanward dipping layers beneath passive continental margins-their origin and paleoenvironmental significance. Geologisches Jahrbuch Reihe E, 3–28

Hinz K, Popovici A, Ronda C, Beisner HD (1988) On a multichannel seismic reconnaissance survey of the Argentine eastern continental margin by R/V xplora. Bundesantalt fur Geowissenschaften und Rohsthoffe, Hannover, Internal Report 102.371, 66 p

Hinz K, Neben S, Schreckenberger B, Roeser HA, Block M, Souza KGD, Meyer H (1999) The Argentine continental margin north of 48 S: sedimentary successions, volcanic activity during breakup. Mar Pet Geol 16:1–25

Hirsch KK et al (2009) Deep structure of the western South African passive margin-results of a combined approach of seismic, gravity and isostatic investigations. Tectonophysics 470:57–70. https://doi.org/10.1016/j.tecto.2008.04.028

Introcaso A (2003) Significativa descomposicón isostática en la Cuenca del Colorado (República Argentina). Rev Asoc Geol Arg 58(3):474–478

Jackson MPA, Cramez C, Fonck JM (2000) Role of subaerial volcanic rocks and mantle plumes in creation of South Atlantic margins: implications for salt tectonics and source rocks. Mar Pet Geol 17:477–498

Jokat W, Boebel T, König M, Meyer U (2003) Timing and geometry of early Gondwana breakup. J Geophys Res 108(B9):2428. https://doi.org/10.1029/2002JB001802

Ludwig WJ, Carpenter G, Houtz RE, Lonardi AG, Ríos FF (1978) Sediment isopach map of the Argentine Continental Margin, Argentine Shelf, Argentine Basin and Falkland Plateau. American Association of Petroleum Geologists, Tulsa, Oklahoma 74101

McKenzie DP (1978) Some remarks on the development of sedimentary basins, Earth planet. Sci Lett 40:25–32

Mckenzie D (1984) A possible mechanism for epeirogenic uplift. Nature 307:616–618

Maclennan J, Lovell B (2002) Control of regional sea level by surface uplift and subsidence caused by magmatic underplating of Earth's crust. Geology 30:675–678. https://doi.org/10.1130/0091 7613(2002)030%3c0675:CORSLB%3e2.0.CO;2

Menzies MA, Klemperer SL, Ebinger CJ, Baker J (2002) Characteristics of volcanic rifted margins. In: Menzies MA, Klemperer SL, Ebinger CJ, Baker J (eds) Volcanic rifted margins. Geological Society of America Special Paper 362, Boulder, pp 1–14

Morgan WJ (1971) Convection plumes in the lower mantle. Nature 230:42–43

Neben A, Franke D, Hinz K, Schreckenberger B, Meyer H, Roeser HA (2002) Early opening of the South Atlantic: pre-rift extension and episodicity of seaward dipping reflector sequence (SDRS), emplacement on the conjugate Argentine amd Namibia continental margins. AAPG Hedberg Conference: Hydrocarbon Habitat of Volcanic Rifted Passive Margins. Stavanger, Noruega. Actas

Nürnberg D, Müller RD (1991) The tectonic evolution of the South Atlantic from Late Jurassic to present. Tectonophysics 191:27–53

Parker C, Paterlini M, Violante RA (1996) Compilación de datos sísmicos y determinación de isopacas en el Mar Argentino. Unpublished work, contribution to the Geological Map of the Argentine Republic

Pedraza De Marchi AC (2015) Caracterización isostática del sector volcánico del margen continental argentino, PhD Thesis. Facultad de Ciencias Astronómicas y Geofísicas, Universidad Nacional de La Plata, La Plata, p 174

Pedraza De Marchi AC, Tocho C, Ghidella M (2012) Comparación de anomalías de gravedad derivadas de altimetría satelital con datos de gravedad marina en el margen continental argentino. Boletim de Ciencias Geodésicas 18(1):22–39

Pedraza De Marchi AC, Ghidella M, Tocho C (2017) 3D process oriented gravity modelling of the Argentine continental margin. J S Am Earth Sci. https://doi.org/10.1016/j.jsames.2017.11.015

Pérez-Gussinyé M, Lowry MR, Watts AB (2007) Effective elastic thikness of South America and its implications for intracontinental deformation. Geochem Geophys Geosyst 8:Q05009. https://doi.org/10.1029/2006gc001511

Rabinowitz PD, Labrecque JL (1979) The Mesozoic South Atlantic Ocean and evolution of its continental margins. J Geophys Res 84:5973–6002

Richards MA, Duncan RA, Courtillot VE (1989) Flood basalts and hotspot tracks: plume heads and tails. Science 246:103–107

Royden L, Keen CE (1980) Rifting process and thermal evolution of the continental margin of Eastern Canada determined from subsidence curves, Earth planet. Sci Lett 51:343–361

Scheck-Wenderoth M, SAMPLE Group (2011) South Atlantic margin processes and links with onshore evolution. AAPG European Region Newsletter, September 2010

Sandwell DT, Smith WHF (1997) Marine gravity from Geosat and ERS 1 satellite altimetry. J Geophys Res 102(B5):10039–10054

Sandwell DT, Smith WHF, Gille S, Steven J, Khalid S, Coakley B (2001) Bathymetry from Space: white paper in support of a higth-resolution, ocean altimeter mission, Sandwell 2001 Bathymetry FS. https://topex.ucsd.edu/

Schnabel M, Franke D, Engels M, Hinz K, Neben S, Damm V, Grassmann S, Pelliza H, Dos Santos PR (2008) The structure of the lower crust at the Argentine continental margin, South Atlantic at 44S. Tectonophysics 454:14–22

Shuman TK (2002) The hydrocarbon potential of the deep offshore along the Argentine volcanic rifted margin. A numerical simulation. PhD Thesis, RWTH, Aarchen Univ., Aarchen Germany, p 194

Stewart J, Watts AB, Bagguley JG (2000) Three-dimensional subsidence analysis and gravity modelling of the continental margin offshore Namibia. Geophys J Int 141:724–746

Talwani M, Abreu V (2000) Inferences regarding initiation of oceanic crust formation from the U.S. east coast margin and conjugate South Atlantic margins. In: Mohriak W, Talwani M (eds) Atlantic

rifts and continental margins. American Geophysical Union, Washington, DC, pp 211–234

Thybo H, Artemieva IM (2013) Moho and magmatic underplating in continental lithosphere. Tectonophysics 609:605–619

Watts AB (1988) Gravity anomalies, crustal structure and flexure of the lithosphere at the Baltimore Canyon Trough. Earth Planet Sci Lett 89:221–238

Watts AB (2001a) Isostasy and flexure of the lithosphere. Cambridge University Press, New York

Watts AB (2001b) Gravity anomalies, flexure and crustal structure at the Mozanbique riften margin. Mar Pet Geol 18:445–455

Watts AB (2018) The use of objet-oriented and processes-oriented methods for gravity anomaly modelling of sedimentary basins. Geophys J Int 215(2):1474–1482

Watts AB, Fairhead JD (1999) A process-oriented approach to modeling the gravity signature of continental margins. Lead Edge 18:258–263

Watts AB, Ryan WBF (1976) Flexure of the lithosphere and continental margin basins. Tectonophysics 36:25–44

Watts AB, Stewart J (1998) Gravity anomalies and segmentation of the continental margin offshore West Africa, Earth planet. Sci Lett 156:239–252

Watts AB, Rodger M, Peirce C, Greenroyd CJ, Hobbs RW (2009) Seismic structure, gravity anomalies, and flexure of the Amazon continental margin, NE Brazil. J Geophys Res 114:B07103. https://doi.org/10.1029/2008JB006259,1.23

White R, McKenzie D (1989) Magmatism at rift zones: the generation of continental margins and flood basalts. J Geophys Res 94:7685–7729

Wilson JT (1963) Evidence from islands on the spreading of the ocean floor. Nature 197:536–538

Wessel P, Luis JF, Uieda L, Scharroo R, Wobbe F, Smith WHF, Tian D (2019) The generic mapping tools version 6. Geochem Geophys Geosyst 20(11):5556–5564. https://doi.org/10.1029/2019GC008515

Zambrano JJ, Urien VM (1970) Geological outline of the basins in Southern Argentina and their continuation off the Atlantic Shore. J Geophys Res 75(8):1363–1396